Energy loss of charged particles moving in cylindrical tubules

You-Nian Wang
The State Key Laboratory of Materials Modification by Laser, Electron, and Ion Beams, Dalian University of Technology, Dalian 116023, People's Republic of China

Z. L. Mišković
Department of Applied Mathematics, University of Waterloo, Waterloo, Ontario, Canada N2L 3G1
(Received 7 December 2001; published 23 October 2002)

The interactions of charged particles with cylindrical tubules are studied within the framework of the dielectric theory. Elementary excitations on a tubule are modeled by an infinitesimally thin layer of free-electron gas, uniformly distributed over the surface of the tubule. The dielectric function of such a system, obtained from the random-phase approximation, exhibits a dimensional crossover from two-dimensional to one-dimensional electron gas, when the radius of the tubule decreases. Energy loss of a charged particle, moving paraxially in a tubule, can be divided into a single-particle excitation part and a resonant excitation part. It is shown that the resonant excitation modes on a tubule, which dominate the energy loss in the high-velocity regime, are quite different from those in a cylindrical cavity in a solid, described by a bulk dielectric function of the surrounding three-dimensional electron gas.

DOI: 10.1103/PhysRevA.66.042904 PACS number(s): 79.20.Rf, 34.50.Bw, 34.50.Dy

I. INTRODUCTION

Ever since their discovery by Iijima in 1991 [1], carbon nanotubes have been widely studied from various aspects, both theoretically and experimentally. In particular, one of the most fascinating aspects is the interaction of charged particles with carbon nanotubes, which may be relevant for applications in several areas of research and technology. For example, important information about the electronic structure of carbon nanotubes can be obtained using the electron probe techniques, such as the transmission-electron microscopy [2] and the electron energy-loss spectroscopy (EELS) [3,4]. On the other hand, in one of the most intriguing applications, carbon nanotubes may be used as waveguides for transporting and focusing charged particle beams [5–9]. In addition, when carbon nanotubes are irradiated by ion beams, their properties and their structure can be modified, resulting in, for example, surface amorphization and diameter shrinkage [10,11].

Theoretical investigation of interactions of charged particles with cylindrical structures by means of the dielectric theory has a rather long history [2,12–17]. Most of the work has been performed for particles moving paraxially through cylindrical cavities (or channels, or capillaries) in the bulk of a solid target [12–16]. In particular, Arista and Fuentes [14–16] have reported pioneering work on the calculations of the induced potentials, energy losses, and the self-energies for ions and clusters moving in microcapillaries and nanocapillaries in solids. On the other hand, Zabala *et al.* [17] have been the first to calculate the energy losses of fast electrons impinging perpendicularly on cylindrical nanowires, made of both metallic and semiconductor materials. It should be pointed out that the structures studied in all those reports [2,12–17] contained solid regions characterized by the bulk dielectric functions for three-dimensional (3D) electron-gas models, which were separated, or bounded, by cylindrical interfaces. The bulk dielectric functions used [2,12–17] were dependent on the frequency only, such as in Drude or Lorentz models, which provided suitable modeling of the high-frequency excitation modes, both in the bulk regions and on the interfaces, in such 3D structures.

Carbon nanotubes present systems that are quite different from the cavities in solids or nanowires made of different materials. Although all these systems share the same underlying cylindrical geometry, carbon nanotubes cannot be modeled as a part of a 3D structure. It is well known that, in general, the dielectric functions of nanotubes exhibit rather rich and complex properties regarding the dependence on the longitudinal wave number, the frequency, and the angular momentum of the elementary excitations, in ways that are strongly influenced by the geometric structure of the nanotube, such as its radius and the chiral angle [18–23]. In a first approximation, elementary excitations on a nanotube may be modeled by an infinitesimally thin layer of free-electron gas, uniformly distributed over an infinitely long cylindrical surface of a tubule. At zero temperature, such an electron gas is completely parametrized by its surface density and the radius of the tubule. Consequently, the dielectric properties of such a system cannot be deduced as a ''zero-thickness limit'' of a cylindrical layer, or film, of a 3D electron gas parametrized by its volume density. This is clearly corroborated by a demonstration that the dielectric function of the free-electron gas on a tubule, obtained in the random-phase approximation (RPA), exhibits a dimensional crossover from a 2D system to a 1D system when the radius of the tubule decreases [18,19].

Therefore, analysis of the interactions of charged particles with nanotubes requires an extension of the formalism developed in the previous studies [2,12–17], in order to fully take into account the complexity of the dielectric response of such a system. Important contribution in that direction has been recently reported by Stöckli *et al.* [24], who have described the dielectric properties of carbon nanotubes by means of the hydrodynamic theory of plasmon excitations in a 2D electron gas on a cylindrical surface, in order to interpret the EELS data for collective excitations on single-wall carbon nanotubes, caused by the incidence of fast electrons perpendicular

to the nanotube. Given the properties of the hydrodynamic model, such a study is suitable for describing the high-energy electrons passing through, or close by, the carbon nanotubes. On the other hand, experimental study of transport, or channeling, of charged particles through carbon nanotubes in the paraxial direction seems feasible, at present, only in the systems of the so-called ''ropes,'' or bunches, of nanotubes [9]. In such systems, the interactions of charged particles with the medium may be described, in a first approximation, by the model of a cylindrical cavity in the bulk of a solid [14–16]. Although the transport of charged particles through single, isolated carbon nanotubes still presents an experimental challenge, we nevertheless address theoretically this problem here in order to elucidate the significance of those dielectric properties of the cylindrical tubules related to the reduced dimensionality of the electron gas, and to compare the results for the energy losses of particles in tubules with those obtained in the cylindrical cavities.

We use, and extend, the dielectric formalism developed by the previous authors for cylindrical structures [2,12–16], in order to study the energy loss of a charged particle moving paraxially inside a tubule characterized by the appropriate RPA dielectric function [18,19], as described above. General expressions for the induced potential and the energy loss of the projectile are presented in Sec. II, which is followed by a discussion of resonant excitations on a tubule in Sec. III, based on the full RPA dielectric function [18,19]. In Sec. IV, we analyze the contributions to the energy loss, coming from the single-particle excitations and the resonant excitations, and present the results of numerical calculations for the total energy loss as a function of the projectile velocity, its position in the tubule, as well as of the radius of the tubule. A short summary is given in Sec. V. Atomic units (a.u.) are used throughout, unless otherwise indicated.

II. GENERAL EXPRESSIONS

We model a tubule as an infinitesimally thin and infinitely long cylindrical shell with the radius a, and assume that the valence electrons can be considered a free-electron gas distributed uniformly over the cylindrical surface. We further consider a charged particle, moving within the tubule, with its trajectory parallel to the tubule axis z, such that the particle's instantaneous position is given in the cylindrical coordinates by $\mathbf{r}_0=(\rho_0,\phi_0,vt)$, where v is the particle's speed. The electric potential $\Phi(\mathbf{r},t)$, created by the particle, can be determined by the Poisson equation

$$\nabla^2\Phi=-4\pi Q\delta(\mathbf{r}-\mathbf{r}_0), \tag{1}$$

where Q is the particle charge.

Taking into account the natural boundary conditions at $\rho=0$ and $\rho=\infty$, Eq. (1) can be solved in cylindrical coordinates $\mathbf{r}=(\rho,\phi,z)$, so that the potential inside the tubule is given by

$$\Phi_1(\rho,\phi,z,t)=\frac{Q}{|\mathbf{r}-\mathbf{r}_0|}+\frac{Q}{\pi}\sum_{m=-\infty}^{\infty}\int_{-\infty}^{\infty}dk e^{ikz+im(\phi-\phi_0)-i\omega t}\times A_m(k,\omega)I_m(k\rho), \tag{2}$$

where $I_m(x)$ is the modified Bessel function of the first kind and $\omega=kv$. The first term in Eq. (2) is the external potential of the moving particle, while the second term is the induced potential. In terms of a Fourier-Bessel expansion, the external potential can be expressed as [25]

$$\frac{Q}{|\mathbf{r}-\mathbf{r}_0|}=\frac{Q}{\pi}\sum_{m=-\infty}^{\infty}\int_{-\infty}^{\infty}dk e^{ikz+im(\phi-\phi_0)-i\omega t}\times I_m(k\rho_<)K_m(k\rho_>), \tag{3}$$

where $\rho_<$ ($\rho_>$) is the smaller (larger) of ρ and ρ_0, and $K_m(x)$ is the modified Bessel function of the second kind. Similarly, the potential outside the tubule can be expressed as

$$\Phi_2(\rho,\phi,z,t)=\frac{Q}{\pi}\sum_{m=-\infty}^{\infty}\int_{-\infty}^{\infty}dk e^{ikz+im(\phi-\phi_0)-i\omega t}\times B_m(k,\omega)K_m(k\rho). \tag{4}$$

The unknown coefficients A_m and B_m in Eqs. (2) and (4) can be determined by the continuity conditions at $\rho=a$, for each angular momentum m. Using the continuity of the electric potential at $\rho=a$ and Eqs. (1)–(4), it is easy to obtain the first relation between A_m and B_m:

$$I_m(k\rho_0)K_m(ka)+A_m(k,\omega)I_m(ka)=B_m(k,\omega). \tag{5}$$

The second relation between A_m and B_m can be obtained by considering the continuity of the displacement field at the tubule's surface:

$$I_m(k\rho_0)K_m'(ka)+A_m(k,\omega)I_m'(ka)=\varepsilon(m,k,\omega)B_m(k,\omega)K_m'(ka), \tag{6}$$

where $\varepsilon(m,k,\omega)$ is the dielectric function of the electron gas on the tubule.

With the above equations, the induced potential inside the tubule can be written as

$$\Phi_{ind}(\rho,\phi,z,t)=\frac{Q}{\pi}\sum_{m=-\infty}^{\infty}\int_{-\infty}^{\infty}dk e^{ik(z-vt)+im(\phi-\phi_0)}\times I_m(k\rho)I_m(k\rho_0)\frac{X_m(k,\omega)}{Z_m(k,\omega)}, \tag{7}$$

in terms of the auxiliary functions

$$X_m(k,\omega)=[1-\varepsilon(m,k,\omega)]K_m(ka)K_m'(ka) \tag{8}$$

and

$$Z_m(k,\omega)=\varepsilon(m,k,\omega)I_m(ka)K_m'(ka)-I_m'(ka)K_m(ka). \tag{9}$$

Finally, using the induced potential, one can obtain the energy loss of the charged particle moving in the tubule, as follows:

$$S=-Q\frac{\partial}{\partial z}\Phi_{ind}(\rho,\phi,z,t)|_{\mathbf{r}=\mathbf{r}_0}$$

$$=\frac{Q^2}{\pi}\sum_{m=-\infty}^{\infty}\int_{-\infty}^{\infty}dkI_m^2(k\rho_0)\mathrm{Im}\left[\frac{X_m(k,kv)}{Z_m(k,kv)}\right]. \quad (10)$$

We note that the form of Eq. (10), along with Eqs. (8) and (9), is the consequence of the geometry of the problem and, as such, it has been obtained before by other authors studying cylindrical structures [12,14]. However, the additional feature here is the appearance in Eqs. (8) and (9) of the dielectric function $\varepsilon(m,k,\omega)$, which depends on the angular momentum m, the longitudinal wavenumber k, and the frequency ω of the elementary excitations on the surface of tubule of radius a, whereas the previous studies [12,14] used in that place in Eqs. (8) and (9) the bulk dielectric function of the surrounding medium, $\varepsilon(\omega)$, which depends on the frequency of elementary excitations in a 3D electron gas.

III. DIELECTRIC FUNCTION AND RESONANT EXCITATIONS

We discuss the properties of the electron gas on a tubule and provide some details regarding the dielectric function used in the present work. It should be mentioned that, when the tubule radius a is large enough, the dielectric behavior of the electron gas on the tubule will be reduced to that of a planar 2D electron gas. On the other hand, for sufficiently small a, the electron gas becomes a 1D system, which is similar to a quantum wire. When the tubule radius a is in the intermediate region, the electron gas on the tubule surface is neither 1D nor 2D system [18,19].

Based on the random-phase approximation, the dielectric function of the tubule can be expressed as [18,19]

$$\varepsilon(m,k,\omega)=1-V(m,k,a)\chi(m,k,\omega), \quad (11)$$

where $V(m,k,a)$ is the Fourier transform of the Coulomb interaction among two electrons on the tubule's surface,

$$V(m,k,a)=4\pi I_m(ka)K_m(ka). \quad (12)$$

Here, $\chi(m,k,\omega)$ is the response function,

$$\chi(m,k,\omega)=\sum_{l=-m_{\max}}^{m_{\max}}\chi(l,m,k,\omega), \quad (13)$$

with

$$\mathrm{Re}\,\chi(l,m,k,\omega)=\frac{1}{2\pi^2 k}\ln\left|\frac{\omega^2-E_-^2(l,m,k)}{\omega^2-E_+^2(l,m,k)}\right| \quad (14)$$

and

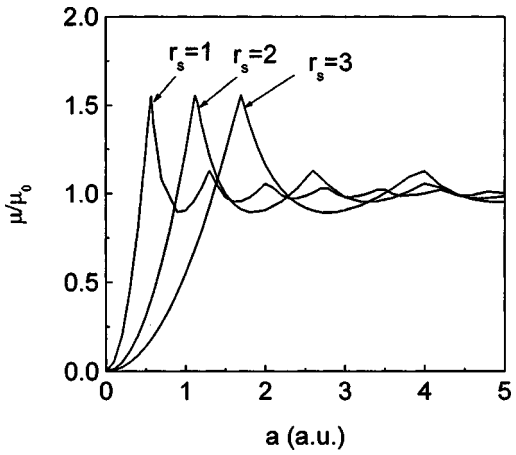

FIG. 1. Dependence of the reduced chemical potential μ/μ_0 on the radius of tubule, a, for several values of the electron density parameter r_s.

$$\mathrm{Im}\,\chi(l,m,k,\omega)=\frac{1}{2\pi k}\ \text{ for }\ |E_-(l,m,k)|<\omega<|E_+(l,m,k)|$$

$$=-\frac{1}{2\pi k}\ \text{ for }\ |E_+(l,m,k)|<\omega<|E_-(l,m,k)|$$

$$=0\ \text{ otherwise.} \quad (15)$$

In the above expressions, $m_{\max}$ is the largest occupied subband index, while

$$E_\pm(l,m,k)=\frac{k^2\pm 2k_F(l)k}{2}+\frac{m^2+2ml}{2a^2}, \quad (16)$$

with $k_F(l)=(2\mu-l^2/a^2)^{1/2}$ being the Fermi momentum of the lth subband, where μ is the chemical potential of the electron gas. For a fixed surface density n_S of the electron gas on tubule, the chemical potential and the largest occupied subband index are related via [18]

$$\frac{\pi^2 a n_S}{\sqrt{2}}=\mu^{1/2}+2\sum_{m=1}^{m_{\max}}\left(\mu-\frac{m^2}{2a^2}\right)^{1/2}, \quad (17)$$

where $m_{\max}=\max[m\,|\,\mu-m^2/(2a^2)>0]$. Figure 1 shows the ways how the reduced chemical potential μ/μ_0 (where $\mu_0=k_F^2/2$ is the chemical potential of a planar 2D electron gas, with $k_F=\sqrt{2\pi n_S}$ being the corresponding Fermi wave number) depends on the tubule radius a, for several values of the electron-density parameter $r_s=(1/\pi n_S)^{1/2}$. One can observe that, when $a<r_s/\sqrt{\pi}$, the chemical potential increases with increasing tubule radius a, so that only the $m=0$ band is occupied. In this case, the electron gas can be regarded as a quasi-1D system. For $a>r_s/\sqrt{\pi}$, however, the chemical potential oscillates around the value characteristic of the planar 2D electron gas, and approaches it as $a\to\infty$.

According to Eq. (15), the imaginary part of the response function $\chi(m,k,\omega)$ becomes zero for high enough frequency ω, giving rise to vanishing of the imaginary part of the func-

tion $Z_m(k,\omega)$, Eq. (9). One can see from Eqs. (7) and (10) that the resonant excitation will occur if the real part of the function $Z_m(k,\omega)$ is zero as well. Thus, the dispersion relation of the resonant excitation modes, $\omega=\omega_m(k)$, is given by the roots of the equation $\mathrm{Re}\,Z_m(k,\omega)=0$, i.e.,

$$\mathrm{Re}\{\varepsilon(m,k,\omega)\}I_m(ka)K_m'(ka)-I_m'(ka)K_m(ka)=0. \tag{18}$$

On combining Eq. (18) with Eq. (11), we obtain the resonance condition

$$\sum_{l=-m_{\max}}^{m_{\max}} \ln\left|\frac{\omega^2-E_-^2(l,m,k)}{\omega^2-E_+^2(l,m,k)}\right|=H_m(k), \tag{19}$$

in terms of the function

$$H_m(k)=\frac{\pi k}{2}\frac{1-g_m(ka)}{I_m(ka)K_m(ka)}, \tag{20}$$

with

$$g_m(x)=1+\frac{1}{xI_m(x)K_m'(x)}, \tag{21}$$

where the Wronskian property, $I_m'(x)K_m(x)-I_m(x)K_m'(x)=1/x$, has been used [26]. When $\omega>|E_\pm^2(l,m,k)|$, one can expand the left-hand side of Eq. (19) to the first order in large ω^2 and obtain the dispersion relation for a tubule as follows:

$$\omega^2\approx\omega_m^2(k)=\frac{4I_m(ka)K_m(ka)}{\pi a^2[1-g_m(ka)]}\times\sum_{l=-m_{\max}}^{m_{\max}}(k^2a^2+m^2+2ml)k_F(l). \tag{22}$$

It is evident from Eq. (22) that the dispersion relation is completely parametrized by the radius of the tubule a and the surface electron-density parameter r_s. In order to provide realistic estimates for the ranges of values of these parameters, we note that the radii of single-wall carbon nanotubes range from about 6.6 to almost 20. Using the atomic density of a graphene sheet, 0.107, the surface electron density of a single-wall carbon nanotube can be approximated by $n_S=4\times0.107$ [27], which yields $r_s=0.86$. In the following, we will present results of our calculations with the a and r_s values close to, or within, such a parameter space. Figure 2 shows the dependences of the resonant frequency modes $\omega_m(k)$ on the longitudinal wave number k for a tubule characterized by $a=10$ and $r_s=0.86$. It should be noticed from the figure that, for $k\to0$, one has $\omega_0(0)=0$, but $\omega_m(0)\neq0$ for $m\neq0$, whereas, for $k\to\infty$, $\omega_m(k)$ approach same function for all m. Actually, the $m=0$ case is quite similar to the plasma dispersion, $\omega(k)=\sqrt{2\pi n_S k}$, in a planar 2D electron gas with the surface density n_S [28].

In order to test how reliable is the modeling of the dielectric function, presented in this section, we consider the experimental data for the dispersion relation of the $\sigma+\pi$ plasmon (the collective excitation of all valence electrons),

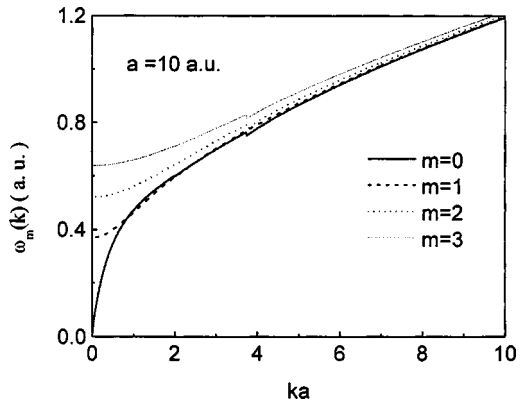

FIG. 2. Dispersion curves $\omega_m(k)$, Eq. (22), for the resonant excitations with several angular-momentum modes m, for a tubule with the radius $a=10$ and the electron-density parameter $r_s=0.86$.

obtained by Pichler and co-workers [3,29]. Those authors have used the EELS technique to measure the loss function $\mathrm{Im}[-1/\varepsilon(m,k,\omega)]$ in bulk samples of purified single-wall nanotubes with $a=0.7$ nm, which is then used to deduce the plasmon dispersion relation. In this case, the resonance condition is $\mathrm{Re}\,\varepsilon(m,k,\omega)=0$, which, on using Eqs. (11)–(14), gives the approximate plasmon dispersion relation as follows:

$$\omega_m^2(k)=\frac{4I_m(ka)K_m(ka)}{\pi a^2}\sum_{l=-m_{\max}}^{m_{\max}}(k^2a^2+m^2+2ml)k_F(l), \tag{23}$$

in analogy to Eq. (22). Note that the dispersion relations in Eqs. (22) and (23) are different because they were derived from resonance conditions being imposed on different functions, $\mathrm{Im}[-1/Z_m(k,\omega)]$ in Eq. (10), and the loss function $\mathrm{Im}[-1/\varepsilon(m,k,\omega)]$, respectively. Figure 3 shows comparison of our theoretical results for $\omega_m(k)$, Eq. (23), with the experimental data of Pichler and coworkers for several excitation modes m. Rather satisfactory qualitative agreement is

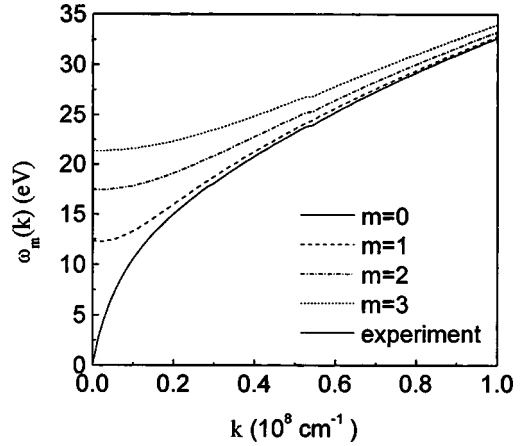

FIG. 3. Comparison of the dispersion curves for the plasmon excitation modes, Eq. (23), with the experimental data, Refs. [3,29], for a carbon nanotube with the radius $a=0.7$ nm and the electron-density parameter $r_s=0.86$.

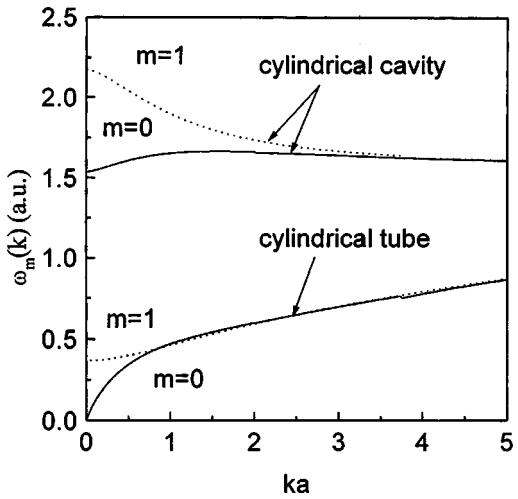

FIG. 4. Comparison of the dispersion curves for the resonant excitation modes $m=0$ and 1 for a cylindrical tubule, Eq. (22), and a cylindrical cavity, Eq. (24), with equal radii $a=10$. The electron-density parameters are equal to 0.86 for both systems (see text).

evident in Fig. 3, which lends confidence in the present modeling of the dielectric function of carbon nanotubes, at least when the collective electron excitations are considered.

Finally, we wish to discuss the relation of the present dielectric model to that used in modeling the cylindrical cavities in solids. Note that the dispersion relation for the resonant mode of a cylindrical cavity in a solid can be deduced from Eq. (18) by replacing the dielectric function $\varepsilon(m,k,\omega)$ of the tubule with the bulk dielectric function of the solid surrounding the cavity [2,14]. Adequate description of a cavity has been achieved [2,14] by using the Drude dielectric function, $\varepsilon(\omega)=1-\omega_p^2/\omega(\omega+\gamma)$, where $\omega_p=\sqrt{4\pi n_V}$ is the plasma frequency of the surrounding 3D electron gas with the volume density n_V, while γ is the damping constant, such that $\gamma \ll \omega_p$. On using the Drude dielectric function in Eq. (18), one recovers the result of the previous authors [2,14] for the plasmon dispersion in a cylindrical cavity of radius a,

$$\omega_m(k)=\omega_p\sqrt{kaI_m(ka)|K_m'(ka)|}. \tag{24}$$

We compare in Fig. 4 the resonant excitation modes $m=0$ and 1 on a cylindrical tubule and in a cylindrical cavity with the equal radii $a=10$, by showing the dispersion curves $\omega_m(k)$ against the reduced longitudinal wave number ka, obtained from Eqs. (22) and (24), respectively. We note that, since the density parameters of the two systems are defined in different ways, i.e., $r_s=(\pi n_S)^{-1/2}$ for the electron gas on the tubule and $r_v=(4\pi n_V/3)^{-1/3}$ for the 3D electron gas surrounding the cavity, we have set $r_s=r_v=0.86$ in Fig. 4 in order to make the physical parameters of the systems comparable. One observes rather striking differences between the two sets of dispersion curves, which are the consequence of the different dimensions of the electron-gas models used to represent the two systems. Consequently, significant differences are expected between the energy losses of charged particles due to resonant excitations in tubules and cavities.

IV. NUMERICAL RESULTS FOR ENERGY LOSS

Using the dielectric function given in Eq. (11), the energy loss, given by Eq. (10), can be divided into two parts: one coming from the single-particle excitations, in which $\mathrm{Im}\,\varepsilon(m,k,\omega)\neq 0$, and the other corresponding to the resonant, or collective, excitations in which $Z_m(k,\omega)=0$. For the single-particle excitations, the energy loss can be calculated directly from Eq. (10), as follows:

$$S_{sp}=\frac{Q^2}{\pi}\sum_{m=-\infty}^{\infty}\int_{-\infty}^{\infty}dkI_m^2(k\rho_0) \times\frac{X_{mi}(k,kv)Z_{mr}(k,kv)-X_{mr}((k,kv)Z_{mi}(k,kv))}{Z_{mr}^2(k,kv)+Z_{mi}^2(k,kv)}, \tag{25}$$

where the subscripts r and i denote the real parts and the imaginary parts, respectively, of the functions $X_m(k,kv)$ and $Z_m(k,kv)$. On the other hand, on using the limiting procedure

$$\lim_{|Z_{mr}|\to 0}\frac{1}{Z_m(k,\omega)}=\lim_{|Z_{mr}|\to 0}\frac{1}{Z_{mr}(k,\omega)-i|Z_{mi}(k,\omega)|} =P[1/Z_{mr}(k,\omega)]+i\pi\delta[Z_{mr}(k,\omega)], \tag{26}$$

one can obtain the resonant excitation part of the energy loss as follows:

$$S_r=Q^2\sum_{m=-\infty}^{\infty}\int_{-\infty}^{\infty}dkI_m^2(k\rho_0)X_{mr}(k,\omega)\left|\frac{\partial Z_{mr}(k,\omega)}{\partial\omega}\right|^{-1} \times[\delta(\omega-\omega_m(k))-\delta(\omega+\omega_m(k))], \tag{27}$$

where $\omega=kv$. Using the resonance condition $Z_{mr}(k,\omega)=0$, along with the expressions for the functions $X_{mr}(k,\omega)$ and $Z_{mr}(k,\omega)$, Eqs. (8) and (9), we finally obtain the resonant energy loss

$$S_r=Q^2\sum_{m=-\infty}^{\infty}k_m^2I_m^2(k_m\rho_0)\frac{K_m(k_ma)}{I_m(k_ma)}, \tag{28}$$

where k_m is a function of the speed v, which is determined by solving the equation $\omega_m(k)=kv$ for each v. The form of Eq. (28) is identical to that obtained by Arista and Fuentes [14], where it represents the total stopping force, since the single-particle contribution S_{sp} is absent due to their use of the k-independent dielectric function $\varepsilon(\omega)$. In addition, the resonant excitations in the two approaches, although described by the same expression, Eq. (28), will give different contributions to the energy loss, owing to the fact that the equation $\omega_m(k)=kv$ is to be solved with different dispersions, given by Eq. (22) or Eq. (24).

In the following calculations, we assume the charged particle to be proton, $Q=1$. The single-particle excitation part S_{sp}, the resonant excitation part S_r, and the total energy loss $S_t=S_{sp}+S_r$ are shown in Figs. 5(a) and 5(b) versus the proton speed v, for two rather small values of the radius of the

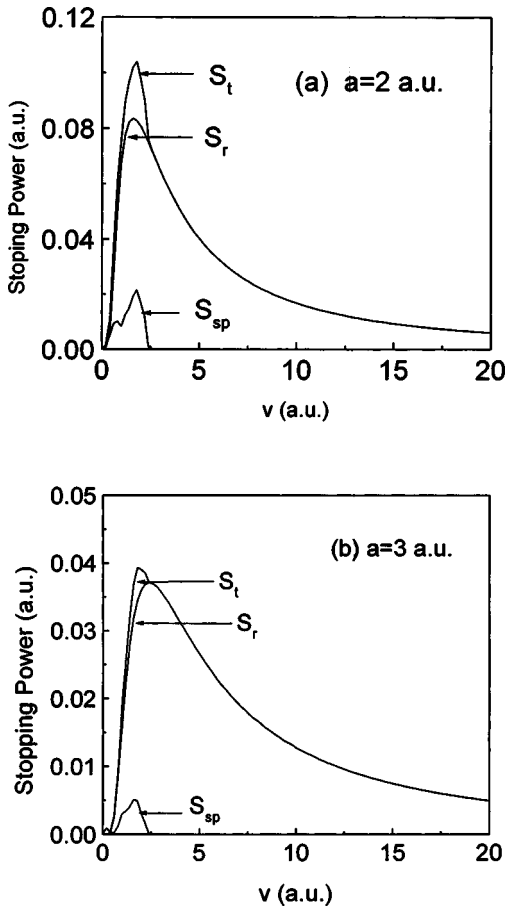

FIG. 5. Energy losses per unit path length versus the speed for a proton that moves in the center, $\rho_0=0$, of tubules with the electron-density parameter $r_s=0.86$, for two values of the radius: (a) $a=2$, (b) $a=3$. S_{sp}, S_r, and S_t describe, respectively, the single-particle excitation part, the resonant excitation part, and the total stopping power.

tubule, $a=2$ and $a=3$, with the particle position $\rho_0=0$ and the electron-gas density parameter $r_s=0.86$. It is clear that the single-particle excitation part S_{sp} is significant only in the low-velocity regime, while the high-velocity regime is dominated by the resonant excitations S_r. It is also clear that the relative participation of the single-particle part S_{sp} in the total energy loss S_t decreases with increasing radius a, so that, for realistic values of a, the stopping seems to be completely dominated by the resonance excitations. Therefore, in Fig. 6, we show the velocity dependence of the resonant stopping power of ions moving at $\rho_0=0$ in tubules with $r_s=0.86$ for several realistic values of the radius, $a=5$, 10, and 15. It is evident from both Fig. 5 and Fig. 6 that the overall magnitude of the ion energy loss decreases, while the maximum of the stopping power shifts to higher speeds v, with increasing radius a of the tubule.

In Fig. 7, we show the influence of the charged particle position ρ_0 on the dependence of the total energy loss on speed, for $a=10$ and $r_s=0.86$. For a fixed speed, the energy loss is smallest when the particle moves along the tubule axis and increases gradually when the particle position shifts closer to the surface of the tubule. One also observes that

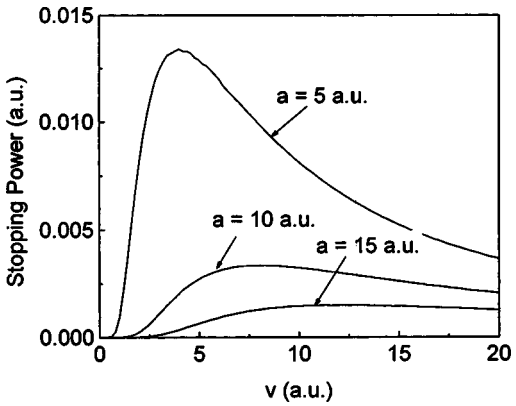

FIG. 6. Velocity dependence of the energy losses per unit path length due to resonant excitations for a proton that moves in the center, $\rho_0=0$, of tubules with the electron-density parameter $r_s=0.86$, for several values of the radius: $a=5$, 10, and 15.

each curve for the energy loss has a maximum, which shifts to a lower speed as the ion moves closer to the surface. Moreover, the role of the single-particle excitations becomes increasingly noticeable at low speeds as the particle moves closer to the surface, even in a tubule with a large radius, such as $a=10$. Finally, we display in Fig. 8 the influence of the density parameter r_s on the dependence of the energy loss on speed, for $a=5$ and $\rho_0=0$. It is observed that, with the increasing density parameter, the positions of the maxima in the energy-loss curves move towards lower speeds, with the peak heights remaining almost unchanged, while the overall shapes of the energy-loss curves become narrower.

V. CONCLUSIONS

We have used the dielectric formalism to study the energy loss of charged particles moving parallel to the axis in cylindrical tubules. On modeling the elementary excitations on the tubule by a free-electron gas confined to the surface of a cylinder, the random-phase approximation gives a dielectric

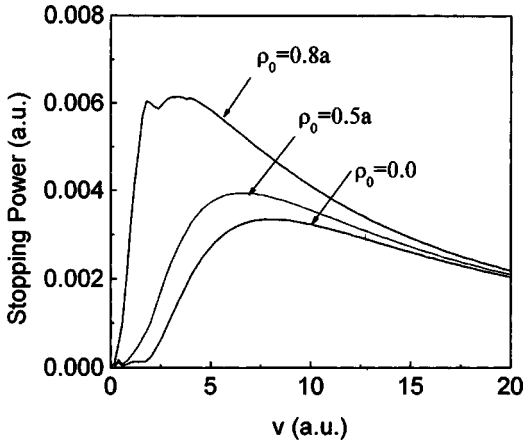

FIG. 7. Total energy loss per unit path length versus the speed for a proton that moves at different positions ρ_0 away from the center of a tubule with the radius $a=10$ and the density parameter $r_s=0.86$.

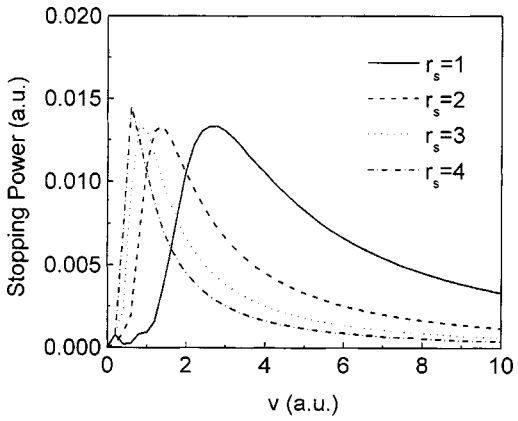

FIG. 8. Total energy loss per unit path length versus the speed for a proton that moves in the center, $\rho_0 = 0$, of a tubule with the radius $a = 5$, for several values of the density parameter r_s.

function that depends on the angular momentum, the wave number, the frequency, and the tubule geometry. Such a model exhibits significant differences, most notably as regards the dispersion of resonant excitation modes, when compared to the model of a cylindrical cavity in a solid, described by a 3D electron gas with a dielectric function that depends only on the frequency. It has been shown that the energy loss is dominated by the contribution from the collective excitations, while the single-particle excitation contribution is generally small and exists only in the low-velocity regimes. In addition, it has been demonstrated that the radius of the tubule as well as the particle position strongly affect the energy loss.

We believe that the results obtained illustrate the importance of suitable modeling of the geometric (i.e., the dimensionality) effects on the dielectric properties of carbon nanotubes and, accordingly, on the energy losses of charged particles moving through them. However, one has to go beyond the free-electron gas model in further refinements of the dielectric formalism, in order to take into account the electronic band structure and the exchange-correlation interaction among the electrons in real carbon nanotubes. As a first estimate, one should expect that such refinements may lead to the introduction of the effective Bohr radius and the effective electron mass. In addition, while the present approach only considers the single-wall nanotubes, it would be interesting to consider the energy loss of charged particles moving through carbon nanotubes with multiple walls.

ACKNOWLEDGMENTS

The authors wish to express their gratitude to Professor Néstor R. Arista for his very useful comments on the present work. This work was jointly supported by the National Natural Science Foundation of China (Grant No. 19975008) and the Ministry of Education State of China (Y.N.W.). Support from the Natural Sciences and Engineering Research Council of Canada is also acknowledged (Z.L.M.).

[1] S. Iijima, Nature (London) **354**, 56 (1991).
[2] A. Rivacoba, P. Appell, and N. Zabala, Nucl. Instrum. Methods Phys. Res. B **96**, 465 (1995).
[3] T. Pichler, M. Knupfer, M.S. Golden, J. Fink, A. Rinzler, and R.E. Smally, Phys. Rev. Lett. **80**, 4729 (1998).
[4] M. Knupfer *et al.*, Carbon **37**, 733 (1999).
[5] K. Tökési, L. Wirtz, and J. Burgdörfer, Nucl. Instrum. Methods Phys. Res. B **154**, 307 (1999).
[6] K. Tökési, L. Wirtz, C. Lemell, and J. Burgdörfer, Nucl. Instrum. Methods Phys. Res. B **164**, 504 (2000).
[7] G.V. Dedkov, Nucl. Instrum. Methods Phys. Res. B **143**, 584 (1998).
[8] N.K. Zhevago and V.I. Glebov, Phys. Lett. A **250**, 360 (1998).
[9] L.A. Gevorgian, K.A. Ispirian, and R.K. Ispirian, Nucl. Instrum. Methods Phys. Res. B **145**, 155 (1998).
[10] Y. Zhu, T. Yi, B. Zheng, and L. Cao, Appl. Surf. Sci. **137**, 83 (1999).
[11] A.V. Krasheninnikov *et al.*, Phys. Rev. B **63**, 245405 (2001).
[12] Y.T. Chu *et al.*, Part. Accel. **16**, 13 (1984).
[13] N. Zabala, A. Rivacoba, and P.M. Echenique, Surf. Sci. **209**, 465 (1989).
[14] N.R. Arista and M.A. Fuentes, Phys. Rev. B **63**, 165401 (2001).
[15] N.R. Arista, Phys. Rev. A **64**, 032901 (2001).
[16] N.R. Arista, Nucl. Instrum. Methods Phys. Res. B **182**, 109 (2001).
[17] N. Zabala, E. Ogando, A. Rivacoba, and F.J. García de Abajo, Phys. Rev. B **64**, 205410 (2001).
[18] O. Sato, Y. Tanaka, M. Kobayshi, and A. Hasegawa, Phys. Rev. B **48**, 1947 (1993).
[19] M.F. Lin and Kenneth W.K. Shung, Phys. Rev. B **47**, 6617 (1993).
[20] P.J. Lin-Chung and A.K. Rajagopal, Phys. Rev. B **49**, 8454 (1993).
[21] M.F. Lin, D.S. Chun, C.S. Huang, and Y.K. Lin, Phys. Rev. B **53**, 15 493 (1996).
[22] B. Tanatar, Phys. Rev. B **55**, 1361 (1997).
[23] M.F. Lin and F.L. Shyu, Physica B **292**, 117 (2000).
[24] T. Stöckli, J.M. Bonard, A. Châtelain, Z.L. Wang, and P. Stadelmann, Phys. Rev. B **64**, 115424 (2001).
[25] J. D. Jackson, *Classical Electrodynamics* (Wiley, New York, 1975).
[26] *Handbook of Mathematical Functions*, edited by M. Abramowitz and I. A. Stegun (Dover, New York, 1972).
[27] D. Ostling, D. Tomanek, and A. Rosen, Phys. Rev. B **55**, 13 980 (1997).
[28] Y.N. Wang and T.C. Ma, Phys. Lett. A **200**, 319 (1995).
[29] M. Knupfer, T. Pichler, M.S. Golden, J. Fink, A. Rinzler, and R.E. Smally, Carbon **37**, 733 (1999).